

Structure of a Class I Tagatose-1,6-bisphosphate Aldolase

INVESTIGATION INTO AN APPARENT LOSS OF STEREOSPECIFICITY*[‡]

Received for publication, November 6, 2009, and in revised form, February 28, 2010. Published, JBC Papers in Press, April 28, 2010, DOI 10.1074/jbc.M109.080358

Clotilde LowKam, Brigitte Liotard, and Jurgen Sygusch¹

From the Department of Biochemistry, Université de Montréal, Montréal, Québec H3C 3J7, Canada

Tagatose-1,6-bisphosphate aldolase from *Streptococcus pyogenes* is a class I aldolase that exhibits a remarkable lack of chiral discrimination with respect to the configuration of hydroxyl groups at both C3 and C4 positions. The enzyme catalyzes the reversible cleavage of four diastereoisomers (fructose 1,6-bisphosphate (FBP), psicose 1,6-bisphosphate, sorbose 1,6-bisphosphate, and tagatose 1,6-bisphosphate) to dihydroxyacetone phosphate (DHAP) and D-glyceraldehyde 3-phosphate with high catalytic efficiency. To investigate its enzymatic mechanism, high resolution crystal structures were determined of both native enzyme and native enzyme in complex with dihydroxyacetone-P. The electron density map revealed a (α/β)₈ fold in each dimeric subunit. Flash-cooled crystals of native enzyme soaked with dihydroxyacetone phosphate trapped a covalent intermediate with carbanionic character at Lys²⁰⁵, different from the enamine mesomer bound in stereospecific class I FBP aldolase. Structural analysis indicates extensive active site conservation with respect to class I FBP aldolases, including conserved conformational responses to DHAP binding and conserved stereospecific proton transfer at the DHAP C3 carbon mediated by a proximal water molecule. Exchange reactions with tritiated water and tritium-labeled DHAP at C3 hydrogen were carried out in both solution and crystalline state to assess stereochemical control at C3. The kinetic studies show labeling at both pro-R and pro-S C3 positions of DHAP yet detritiation only at the C3 pro-S-labeled position. Detritiation of the C3 pro-R label was not detected and is consistent with preferential cis-trans isomerism about the C2–C3 bond in the carbanion as the mechanism responsible for C3 epimerization in tagatose-1,6-bisphosphate aldolase.

Aldolases are crucial enzymes in living organisms because of their role in essential metabolic pathways, such as gluconeogenesis and glycolysis. Their ability to control the stereochemistry of the carbon-carbon bond formation makes them models for *de novo* preparation of carbohydrates (1) and ideal alternatives to traditional methods in synthetic organic chemistry

(2–4). Tagatose-1,6-bisphosphate (TBP)² aldolase is an inducible enzyme that, although demonstrating greatest affinity for D-tagatose 1,6-bisphosphate, can also use as substrate the bisphosphorylated D-hexose stereoisomers: sorbose bisphosphate, psicose bisphosphate, and fructose bisphosphate (5). The four sugars are diastereoisomers and differ in stereochemistry at carbon 3 and at carbon 4 with respect to the configuration of their hydroxyl groups. The cleavage of the four sugars produces glyceraldehyde 3-phosphate and dihydroxyacetone phosphate (DHAP), whereas the condensation of glyceraldehyde 3-phosphate and DHAP produces a mixture of the four D-hexoses in *Staphylococcus aureus* (5).

Aldolases are broadly categorized with respect to their catalytic mechanism into two classes. Class I aldolases are characterized by formation of covalent Schiff base intermediates (6–8), whereas class II aldolases are metallodependent enzymes and use a divalent transition metal ion to polarize the substrate ketose (9, 10). Of all aldolases, class I FBP aldolase from rabbit muscle has been the most extensively studied (11, 12). To form the FBP C3–C4 bond in aldol condensation, the enzyme stereospecifically abstracts the pro-S C3 proton of the iminium intermediate formed by a lysine residue in the active site with DHAP (13–15), thereby generating the carbanionic character at C3 of DHAP for the aldol reaction. The nascent carbon-carbon bond has the same orientation as the pro-S α -hydrogen initially abstracted from the DHAP imine intermediate, the carbanion *si* face being subjected to a nucleophilic attack by the *si* face of the incoming glyceraldehyde 3-phosphate aldehyde (16). The iminium intermediate formed is then hydrolyzed, and FBP is released. Similarly, in L-rhamnulose-1-phosphate aldolase, the attack by the *re* face of L-lactaldehyde on the *re* face of DHAP yields rhamulose 1-phosphate (17, 18) and also retains configuration.

Racemic aldol condensation products with respect to the configuration at C4 have been noted in a number of aldolases. In 2-keto-4-hydroxyglutarate aldolase (19) and in L-fuculose-1-phosphate aldolase, racemization occurs at C4 of the condensation products, resulting from random orientation of the aldehyde during stereofacial attack (20) and from its chemical nature (21). In contrast, configuration at both C3 and C4 is not retained in the catalytic mechanism of the class I TBP aldolase from *S. aureus*, given that aldol condensation yields a mixture of sorbose bisphosphate, psicose bisphosphate, fructose bisphosphate, and tagatose bisphosphate (5).³ Attempts

* This work was supported by grants from the Natural Science and Engineering Research Council (Canada) and Canadian Institutes for Health Research (to J. S.).

[‡] The on-line version of this article (available at <http://www.jbc.org>) contains supplemental Fig. S1 and Table S1.

The atomic coordinates and structure factors (codes 3MHF and 3MHG) have been deposited in the Protein Data Bank, Research Collaboratory for Structural Bioinformatics, Rutgers University, New Brunswick, NJ (<http://www.rcsb.org/>).

¹ To whom correspondence should be addressed: CP 6128, Station Centre Ville, Montréal, Québec H3C 3J7, Canada. Tel.: 514-343-2389; Fax: 514-343-6463; E-mail: Jurgen.Sygusch@UMontreal.ca.

² The abbreviations used are: TBP, tagatose 1,6-bis(phosphate); FBP, fructose 1,6-bis(phosphate); DHAP, dihydroxyacetone phosphate; MAD, multiple-wavelength anomalous dispersion; r.m.s., root mean square.

³ This observation was verified for *S. pyogenes* TBP aldolase and is described in the supplemental material.

Structure of a Class I TBP Aldolase

have been made to switch the specificity of class II TBP aldolases; however, these have been met with limited success (22, 23).

Three-dimensional structures of class I FBP aldolases have been determined from different organisms (24–26), and reaction intermediates have been characterized (27), providing a detailed description of the catalytic mechanism at the molecular level, including a structural explanation for stereospecific proton exchange at C3 (11). In sharp contrast, insights into how class I TBP aldolase catalyze racemic aldol condensation products at the molecular level have been hampered by an absence of structures of reaction intermediates. We thus initiated high resolution crystallographic studies of class I TBP aldolase from *Streptococcus pyogenes* in conjunction with isotopic labeling studies to investigate its reaction mechanism and the structural basis for the apparent loss of stereospecificity.

Here, we present the three-dimensional structure of a native class I TBP aldolase as well as its complex with DHAP using TBP aldolase crystals incubated in the presence of DHAP. Flash cooling of a native TBP aldolase crystal soaked in a saturating DHAP solution trapped a covalent reaction intermediate. The structure revealed conformational changes upon binding, whereby the active site undergoes asymmetrical narrowing to grasp DHAP. The location of an invariant water molecule within close contact of the DHAP C3 carbon in the trapped intermediate underscored a stereospecific proton transfer mechanism conserved in Schiff base-forming aldolases.

The extent of stereochemical control in class I TBP aldolases with respect to C3 epimerization was also examined in both solution and crystalline state. Catalytic proton transfer was assessed by the lability of the pro-*R* and pro-*S* C3 hydrogens of DHAP to exchange in tritiated water. The proton exchange studies, in conjunction with the structural data, afforded identification of the carbanion as the dominant steady state reaction intermediate and indicated *cis-trans* isomerism about the carbanion C2–C3 bond in explaining the loss of stereospecific proton exchange at the DHAP C3 carbon in TBP aldolase. These findings stand in contrast to the highly stereospecific proton exchange mechanism found in class I FBP aldolases and point to rotational isomerization in specific reaction intermediates as an evolutionary simple solution capable of generating enantiomeric promiscuity.

EXPERIMENTAL PROCEDURES

Purification and Crystallization—Plasmid pKK-223-3 with T7 isopropyl 1-thio- β -D-galactopyranoside-inducible promoter and coding for the *lacD2* gene product from *S. pyogenes*, tagatose-1–6-bisphosphate aldolase 2, was transformed and overexpressed using the JM109 strain (Promega) in *Escherichia coli*. Recombinant TBP aldolase was purified to homogeneity using a three-step chromatographic protocol as reported previously (28). Briefly, cells were lysed at 4 °C, and the lysate was applied onto an anion exchange column (DEAE-Sepharose Fast Flow) and eluted with a NaCl gradient at pH 7.5. Enzymatic activity was determined by following NADH oxidation at 340 nm using a coupled assay (29). The active fractions were dialyzed overnight against a solution of 1.5 M $(\text{NH}_4)_2\text{SO}_4$, 50 mM NaH_2PO_4 , pH 7.0, and then applied onto a hydrophobic affinity column (phenyl-Sepharose, Amersham Biosciences). TBP

aldolase was eluted using a continuous gradient of NaH_2PO_4 . The active fractions were then dialyzed overnight against a precipitating solution of 90% saturating $(\text{NH}_4)_2\text{SO}_4$, pH 7.0, and then applied after resolubilization onto a size exclusion column (SuperdexTM 200, Amersham Biosciences). The purified protein was precipitated overnight using the same 90% saturated $(\text{NH}_4)_2\text{SO}_4$, pH 7.0 solution as before, and stored at 4 °C. Yields corresponded to ~50 mg of purified enzyme per liter of *E. coli* culture.

TBP aldolase crystals were grown using the hanging drop method, from a 1:1 mixture of protein solution (initial concentration 5 mg/ml in 10 mM Tris-HCl, pH 7.0) and precipitant buffer (9–11% polyethylene glycol 4000 in 0.2 M calcium acetate and 0.1 M Tris-acetic acid, pH 7.5) that was equilibrated against a reservoir of precipitant.

Cleavage Assay—The substrate cleavage rate was determined by measuring the decrease in A_{340}/min using a coupled assay (27). Aldolase was diluted in 50 mM Tris-HCl, pH 7.5, and added to a cuvette containing 50 mM Tris-HCl, pH 7.5, 10 mM EDTA, 0.16 mM NADH, and 10 $\mu\text{g}/\text{ml}$ glycerol-3-phosphate dehydrogenase/triose-phosphate isomerase. Assays (1 ml) were performed in triplicate at 23 °C following the addition of substrate. The cleavage rate for FBP and TBP substrates was measured over a substrate concentration range of 1–5000 μM , using 1 μg of wild type enzyme. TBP aldolase concentration was determined by BCA protein assay reagent (Pierce), with bovine serum albumin serving as a standard.

Data Collection and Processing—TBP aldolase crystals were soaked in DHAP buffer (mother liquor plus 5 mM DHAP) for 5 min. Crystals were then mounted in nylon cryoloops (Hampton Research) after brief immersion in cryoprotectant (mother liquor plus 5 mM DHAP plus 20% glycerol) and then immediately flash-cooled in a nitrogen gas stream at 100 K. Diffraction data were collected at beamline X25 of the National Synchrotron Light Source (Brookhaven National Laboratory, Upton, NY). A native data set was also collected at beamline X29. Data indexing and integration were performed using HKL2000 (30).

MAD Phasing and Refinement—The three-dimensional structure of TBP aldolase from *S. pyogenes* was solved using MAD phasing on previously collected data of a SeMet crystal (28). The three different wavelength (inflection, peak, and remote) MAD data sets allowed the program SOLVE (31) to determine the positions of five selenium atoms of six possible in each protomer and to estimate initial protein phases. Solvent flattening with the program RESOLVE (32) yielded an interpretable electron density map calculated at 2.6 Å resolution. Iterative cycles of chain tracing using O (33) and model refinement using the Crystallography and NMR System (CNS) (34) defined a trace of the polypeptide backbone that refined to R_{cryst} (R_{free}) values of 0.246 (0.290).

Molecular Replacement and Refinement—Native free TBP aldolase crystallized in the $P2_12_12_1$ space group with four protomers in the asymmetric unit and diffracted to 1.87 Å resolution. The structure was solved by molecular replacement using the initial MAD phased model as a search probe. Structure refinement consisted of iterative rounds of simulated annealing and minimization with CNS and Phenix (35) and model building using O and Coot (36). Water molecules were initially

TABLE 1
Data collection and refinement statistics

	Native	DHAP-bound
Data collection		
Resolution	50-1.87 (1.97-1.87) ^a	50-1.92 (2.02-1.92)
Wavelength	0.9795	0.9795
Unique reflections	144,212 (15,756)	142,361 (12,153)
Completeness (%)	74.8 (82.5)	85.9 (74.1)
Average $I/\sigma(I)$	7.1 (1.4)	7.8 (2.9)
R_{sym}^b	0.092 (0.513)	0.101 (0.326)
R^c	0.071 (0.419)	0.045 (0.186)
R_{meas}^d	0.113 (0.650)	0.120 (0.440)
Unit cell parameters <i>a</i> , <i>b</i> , <i>c</i> (Å)	63.7, 106.2, 238.5	64.1, 108.2, 238.7
Refinement		
No. of atoms		
Protein	10,248	10,192
Water	2336	2597
Hetero	7 Ca	7 Ca, 36 DHAP atoms
σ cut-off; $I/\sigma(I) >$	1	1
R_{cryst} (%) ^e	17.5	16.1
R_{free} (%) ^f	21.8	19.9
r.m.s. deviation		
Bond length (Å)	0.005	0.004
Bond angle (degrees)	0.929	0.869
Average <i>B</i> -factor (Å ²)	32.75	22.22
Ramachandran analysis ^g (%)		
Favored	96.3	97.1
Allowed	3.7	2.9

^a Values in parentheses are given for the highest resolution shell.

^b $R_{\text{sym}} = \sum_{hkl} \sum_i |I_i(hkl) - \bar{I}(hkl)| / \sum_{hkl} \sum_i I_i(hkl)$ with *i* running over the number of independent observations of reflection *hkl*.

^c $R_{\text{pim}} = \sum_{hkl} \sqrt{(1/(n-1)) \sum_i (I_i - I_{\text{mean}}) / \sum_{hkl} \sum_i I_i}$.

^d $R_{\text{meas}} = \sum_{hkl} \sqrt{(n/(n-1)) \sum_i (I_i - I_{\text{mean}}) / \sum_{hkl} \sum_i I_i}$.

^e $R_{\text{cryst}} = \sum_{hkl} |F_o(hkl) - |F_c(hkl)|| / \sum_{hkl} |F_o(hkl)|$.

^f $R_{\text{free}} = \sum_{hkl \in T} |F_o(hkl) - |F_c(hkl)|| / \sum_{hkl \in T} |F_o(hkl)|$, where *T* is a test data set randomly selected from the observed reflections prior to refinement. The test data set was not used throughout refinement and contains 7.5% of the total unique reflections for native and native aldolase bound with DHAP.

^g Analyzed by MolProbity (34).

added automatically by CNS and Phenix and by manual addition in subsequent rounds. The final model has in each asymmetric unit cell four protomers of 322 residues each, 2336 water molecules, and 7 cations of calcium.

The liganded crystal structure was isomorphous with the crystal structure of the native aldolase and diffracted to 1.92 Å resolution. Initial phases used for model building of the liganded structure were obtained by molecular replacement using the MAD phased model for the TBP aldolase as a search probe. The polypeptide trace of the liganded structure was determined using the same model building and refinement protocol as described for the native enzyme. DHAP was refined as a covalent intermediate bound to Lys²⁰⁵ in all four protomers.

Structure refinement used all reflections having an $I/\sigma(I) > 1$; however, electron density maps were calculated to the resolution indicated in Table 1 to ensure at least ~80% completeness in the highest resolution shell with an $I/\sigma(I) > 2$. The PRODRG server was used to generate ligand topology and parameter files (37). The presence of ligands in the final models was confirmed by inspection of simulated annealing $F_o - F_c$ omit maps. Final model statistics, calculated with CNS and MolProbity are shown in Table 1. Multiplicity-weighted *R* factors (38) as output by SCALA in CCP4 (39) are also shown in Table 1. The final structure models have R_{cryst} (R_{free}) values of 0.175 (0.218) and 0.161 (0.199), respectively. The corresponding positional errors in atomic coordinates using maximum likelihood plots were estimated to be 0.21 and 0.17 Å, respectively. Errors in hydrogen bond distances and positional differences are reported as

S.D. values and were estimated based on their value in each aldolase protomer unless specified otherwise. Intersubunit variability among the four protomers in the asymmetric unit cell was analyzed by the program Polypose (40) and yielded r.m.s. differences, based on C α atom coordinates, similar to the error in the atomic coordinates for each structure. All figures were prepared using the program PyMOL (41).

Chemical identity of the enzymatic intermediate trapped in the DHAP-TBP aldolase structure was determined with the program O (33), using a simulated annealing omit map. The real space statistic R_{fact} was calculated in O (RS_FIT function) to evaluate the fit of Lys²⁰⁵ N ζ and C ϵ atoms, and DHAP C1, C2, C3, and O3 atoms were modeled as enamine and iminium forms to the electron density. The discrimination between those two chemical species was made using Student's *t* test comparing pairwise R_{fact} statistics in each subunit, with bound DHAP refined as either iminium/carbanion or enamine form (11).

Proton Exchange—Tritium was used as a tracer to measure label incorporation at the DHAP C3 hydrogen catalyzed by TBP aldolase in solution and in crystals. Incorporation of the label at (S)-C3 and (R)-C3 of DHAP was determined using an ion exchange protocol (Dowex Cl⁻ resin) described previously (16). Stereospecific deprotonation at DHAP C3 by rabbit muscle aldolase and triose-phosphate isomerase was used to determine the extent of stereospecific labeling as (S)-[3-³H₁]DHAP and (R)-[3-³H₁]DHAP, respectively (16). Label released as tritiated water (detritiation) was determined as described previously and quantitated to assess epimerization at C3 by TBP aldolase.

DHAP labeled as (S)-[3-³H₁]DHAP or (R)-[3-³H₁]DHAP from tritiated water (tritiation) was prepared using the ability of FBP aldolase and triose-phosphate isomerase to stereospecifically label pro-*S* and pro-*R* C3 positions of DHAP, respectively. Detritiation catalyzed by TBP aldolase in solution and in crystals was followed by the appearance of label as tritiated water from (S)-[3-³H₁]DHAP or (R)-[3-³H₁]DHAP using the same ion exchange protocol. Rates of label exchange were determined under conditions corresponding to initial rate kinetics.

Aliquots of soluble TBP aldolase ranging from 1 to 5 μg made up in 10 mM Tris-HCl, 100 mM NaCl, pH 7.0, were used for the exchange studies. For the tritiation experiments, 20 mM DHAP and 5 mCi of T₂O (average specific activity of 70884 cpm/ μmol) were added to the mixture and incubated for 1–10 min at room temperature. For the detritiation experiments, 4 mM DHAP and 1 mM of DHAP labeled at either the pro-*R* or pro-*S* position of carbon C3 (average specific activity of 2053 cpm/ μmol), were added and incubated for 1–10 min at room temperature. For tritiation and detritiation by TBP aldolase in the crystalline state, crystals were washed three times in fresh mother precipitant solution and then incubated in the same tritiation and detritiation mixtures as was the soluble protein. Quantities of crystalline TBP aldolase used ranged from 38 to 51 μg , and incubation times ranged from 10 min to 4 h. The quantity of crystalline enzyme and incubation time was greater compared with soluble TBP aldolase to ensure sufficient count rates that were significantly above background. Net count rates were calculated by subtracting background count rate measured in the

Structure of a Class I TBP Aldolase

absence of enzyme. Background represented <0.1% of the lowest exchange rate measured in the presence of soluble enzyme and between 25 and 50% of the count rate in the presence of crystalline enzyme. The final assay volume was 1 ml, and 300- μ l aliquots were used for analysis. Exchange rates were measured in triplicate with both soluble and crystalline enzyme.

Kinetic Solvent Isotope Effect—To evaluate D₂O kinetic solvent isotope effects, enzyme activity measurements were performed in D₂O using 50 mM Tris-acetic acid buffer, pH 7.5. The effect of D₂O on pH was corrected for. Substrate and Tris-acetic acid buffer was made up in D₂O, and coupling enzymes were diluted in D₂O prior to usage. Together, this amounted to less than a 5% reduction in D₂O concentration in the activity assay. TBP aldolase was dialyzed against three successive changes of D₂O for at least 1 h until measured activity became stable. Enzyme dialyzed against three similar successive changes of H₂O was used for control.

RESULTS

Native TBP Aldolase—TBP aldolase from *S. pyogenes* exhibits a α/β_8 -triose-phosphate isomerase barrel fold similar to the polypeptide fold observed for rabbit muscle aldolase (24), with which it shares less than 12% sequence identity. The secondary structure elements assigned using PyMOL consist of 11 α -helices and eight β -strands. The native enzyme has four protomers in the asymmetric unit cell, and arrangement of the protomers is best described in terms of two identical dimers. Each dimer interface implicates primarily hydrogen bond interactions between subunit α helices, $\alpha 5$ and $\alpha 6$ of one subunit and the same helices $\alpha 5$ and $\alpha 6$ in the other subunit. The surface buried at the subunit dimer interface represents 1908 \AA^2 , whereas the dimer-dimer interface, constituted by one dimer subunit interacting with the subunit dimer interface of the second dimer, buries 1319 \AA^2 . Calcium ions were located at the dimer-dimer interfaces and participated in bridging interactions. Size exclusion chromatography corroborated the dimeric quaternary structure of TBP aldolase, which elutes at a relative molecular weight of 70,000. A schematic representation of the TBP aldolase dimer with overall dimensions of $\sim 34 \times 36 \times 44$ \AA is shown in supplemental Fig. S1. The dimeric subunits are related by a non-crystallographic 2-fold axis of rotation such that subunit active sites face the same direction.

Carbanion Intermediate—A TBP aldolase crystal soaked in a DHAP solution and flash-cooled trapped a covalent enzymatic intermediate in each of the four subunits in the asymmetric unit that permitted unambiguous identification of the active site. The active site of TBP aldolase is situated deep in the center of the α/β_8 barrel fold, as was observed for rabbit muscle aldolase. Continuous electron density extending from Lys²⁰⁵ N ζ to DHAP C2 shows formation of a stable covalent intermediate (Fig. 1A). The iminium and/or carbanion intermediate can be distinguished from the enamine intermediate because of sp^2 hybridization at Lys²⁰⁵ N ζ , as shown by the planar shape of the electron density observed about the Lys²⁰⁵ N ζ . Furthermore, DHAP O3 points slightly out of the plane defined by Lys²⁰⁵ N ζ and DHAP carbon atoms C1, C2, and C3, which is not possible in the enamine intermediate and is consistent with the trapping of an iminium and/or carbanion intermediate in each TBP

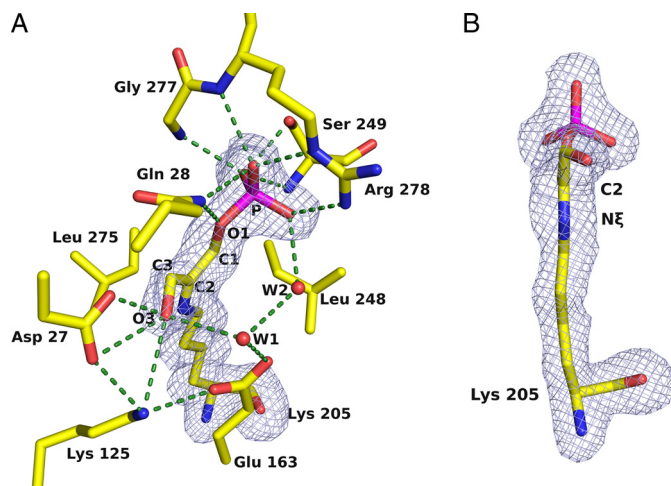


FIGURE 1. A, covalent enzymatic intermediate formed by *S. pyogenes* TBP aldolase with DHAP. DHAP P1 oxyanion makes interactions with Arg²⁷⁸, Gly²⁷⁷, and Ser²⁴⁹, and DHAP C3 via its hydroxyl interacts with Asp²⁷ and Lys¹²⁵. Water molecule Wat¹ (W1) makes close contact with DHAP C3 hydroxyl and hydrogen-bonds with Glu¹⁶³, whereas Wat² (W2) interacts with the DHAP oxyanion and makes close contacts with Wat¹, Glu¹⁶³, and Arg²⁷⁸. Difference electron density was calculated from a 1.92 \AA simulated annealing $F_o - F_c$ omit map encompassing Lys²⁰⁵ and DHAP and contoured at 0.0 σ . B, electron density showing trapping of a carbanion intermediate in the active site of TBP aldolase. Electron density of the enzymatic intermediate was consistent with geometry corresponding to a carbanion and/or iminium species bound in the active site of all subunits of the trapped DHAP-TBP aldolase complex. The covalent intermediate has sp^2 hybridization at Lys²⁰⁵ N ζ and hence planar shape when viewed perpendicular to the plane containing DHAP carbon atoms C1, C2, and C3; additionally, DHAP O3 points out of this plane, corroborating the intermediate identification as a carbanion and/or iminium. Difference electron density was calculated from a 1.92 \AA simulated annealing $F_o - F_c$ omit map encompassing Lys²⁰⁵ and DHAP and contoured at 3.0 σ . Green dashes, hydrogen bonding interactions; red spheres, water molecules.

aldolase subunit (Fig. 1B). Average B -factors of the bound DHAP (16.6 ± 6.2 \AA^2) and of interacting side chains (14.3 ± 5.8 \AA^2) indicate full active site occupancy by DHAP.

To further corroborate the identity of the bound intermediate, the real space R_{fact} statistic was calculated using the O program in order to gauge the model fit to the electron density. The derived Student's t test compared R_{fact} values for DHAP modeled either as an enamine intermediate with planar geometry for DHAP atoms C1, C2, C3, and O3 and sp^3 hybridization at Lys²⁰⁵ N ζ or as an iminium/carbanion intermediate with sp^2 hybridization at Lys²⁰⁵ N ζ and coplanarity for DHAP atoms C1, C2, and C3 only. The statistic was discriminatory with $p = 0.072$, the iminium and/or carbanion showing significantly lower R_{fact} than the enamine in all four subunits.

The DHAP intermediate is engaged in several stabilizing bonds with active site residues. DHAP P1 phosphate hydrogen bonds with Arg²⁷⁸, Gly²⁷⁷, and Ser²⁴⁹; Arg²⁷⁸ curls around and interacts electrostatically with the P1 oxyanion, creating a binding pocket, whereas Gly²⁷⁷ and Ser²⁴⁹ provide three additional hydrogen bonds with the oxyanion. The intermediate is further stabilized by Gln²⁸ hydrogen bonding DHAP O1 and its oxyanion. DHAP C3 via its hydroxyl forms two hydrogen bonds with Asp²⁷ and Lys¹²⁵. A water molecule Wat¹, hydrogen-bonded to Glu¹⁶³, is positioned nearly perpendicular to the plane of the iminium/carbanion and makes *si* face close contact with DHAP C3 hydroxyl (3.34 ± 0.14 \AA). Comparison of B -factors of Wat¹ with those of proximal water molecules suggests

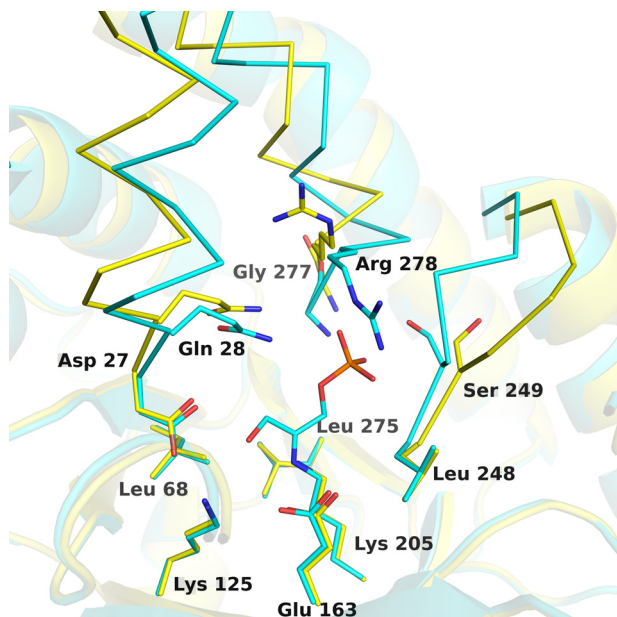


FIGURE 2. Superposition of liganded TBP aldolase structure (cyan) with the native enzyme structure (yellow). Three regions of continuous sequence whose backbones undergo conformational displacement upon DHAP binding are shown in a stick representation. For region 1, residues Asp²⁷ and Gln²⁸ interact with DHAP upon binding, and in region 2, residue Ser²⁴⁹ interacts with DHAP, whereas in region 3, residues Gly²⁷⁷ and Arg²⁷⁸ are shown interacting with the carbanion intermediate. The conformational displacements narrow asymmetrically the active site cavity with respect to the free enzyme.

variable occupancy by Wat¹ in the four protomers. Water molecule Wat² hydrogen-bonds the phosphate oxyanion and makes close contact with Wat¹ and, contrary to Wat¹, shows full occupancy in all protomers. Superposition of the four subunits of the native and DHAP-bound aldolase showed the positions of these two water molecules to be invariant to active site binding.

Conformational Changes and Active Site Binding—Comparison of the four protomers in the asymmetric unit cell of the native TBP aldolase with those of the DHAP bound enzyme yielded r.m.s. deviation values of 0.98 Å using all residues and 0.36 Å when comparing only residues 100–230 delineating the same central domain in each subunit that is invariant to binding events. Superposition of the native and DHAP-bound structures of TBP aldolase defined three regions that underwent systematic conformational changes due to active site binding (Fig. 2). Region 1 (residues 25–50), region 2 (residues 245–250), and region 3 (residues 275–295) contributed residues Asp²⁷ and Gln²⁸, residue Ser²⁴⁹, and residues Gly²⁷⁷ and Arg²⁷⁸, respectively, which interacted with the covalent intermediate, thereby narrowing the active site with respect to the free enzyme. The calculated r.m.s. deviation values between the native and liganded structures corresponding to the rigid body movements of region 1, 2, and 3 were 0.60 ± 0.36 , 0.35 ± 0.10 , and 1.25 ± 0.60 Å, respectively.

Sequence Similarity—A BLAST2 search using *S. pyogenes* TBP aldolase as a search probe yielded high sequence similarity with TBP aldolases from other streptococci, *S. aureus* TBP aldolase (5), and LacD.1, a paralogue of the LacD.2 gene that codes for *S. pyogenes* TBP aldolase, (see supplemental material). Three-dimensional models were built and were successfully

threaded onto the native structure of *S. pyogenes* TBP aldolase (see supplemental material for details). Residues Asp²⁷, Gln²⁸, Arg²⁹, Glu⁹², Lys¹²⁵, Glu¹⁶³, Lys²⁰⁵, Leu²⁷⁵, Gly²⁷⁷, and Arg²⁷⁸, all proximal to the DHAP intermediate in *S. pyogenes* TBP aldolase, were conserved and threaded into identical positions for all structures. The highest scoring structures identified by a structure similarity search using the Dali server (42) were a putative *Salmonella typhimurium* class I Yht aldolase (Protein Data Bank entry 1TO3) and rabbit muscle FBP aldolase in complex with DHAP (Protein Data Bank entry 2QUT). The same spatial disposition of residues Asp²⁷, Gln²⁸, Arg²⁹, Glu⁹², Lys¹²⁵, Glu¹⁶³, Lys²⁰⁵, Leu²⁷⁵, Gly²⁷⁷, and Arg²⁷⁸ in these structures corroborated that the *S. pyogenes* TBP aldolase active site is highly conserved.

Active Site Comparison of Class I TBP and FBP Aldolases—To investigate structural similarity of the TBP and FBP aldolase active sites, superimposition of the DHAP-bound structures of TBP aldolase and of FBP rabbit muscle aldolase (Protein Data Bank entry 2QUT) (11) were performed. The best alignment using Swiss Model (43) corresponded to a match of 148 residues that yielded a calculated r.m.s. deviation of 1.64 Å (based on C α atoms) and revealed extensive homology among active site residues. Finer alignment based on conserved active site residues and DHAP atoms yielded r.m.s. deviation values of 1.06 Å (C α atoms) for active site residues and 0.28 Å for DHAP atoms; the latter r.m.s. deviation value could be further decreased to 0.12 Å when the DHAP O3 atom was excluded. Active site residues interacting and those in close contact with the trapped covalent intermediate, shown in Fig. 3, were largely conserved between the two aldolases. Spatial disposition of active site residues Lys²⁰⁵, Glu¹⁶³, Lys¹²⁵, Asp²⁷, Gly²⁷⁷, Arg²⁷⁸, Ser²⁴⁹, and Leu²⁴⁸, conserved in class I TBP aldolases, was identical with active site residues Lys²²⁹, Glu¹⁸⁷, Lys¹⁴⁶, Asp³³, Gly³⁰², Arg³⁰³, Ser²⁷¹, and Leu²⁷⁰, conserved in class I FBP aldolases. The positions of water molecules, Wat¹ and Wat², were similarly spatially disposed. The only striking difference was the replacement of Ser³⁰⁰ in FBP aldolase by Leu²⁷⁵ in TBP aldolase. The Ser³⁰⁰ hydroxyl in the DHAP bound FBP aldolase structure forms a hydrogen bond with Lys²²⁹ N ζ , thus stabilizing the enamine intermediate (11), which is not possible by Leu²⁷⁵ in TBP aldolase.

Kinetic Characterization—Michaelis-Menten kinetics was used to analyze initial rate velocities measured using FBP and TBP as substrates, and kinetic parameters k_{cat} and K_m are shown in supplemental Table S1. The data show a higher k_{cat} for TBP as substrate than for FBP (13 s^{-1} as opposed to 4 s^{-1}) and a lower K_m for TBP than for FBP (543 and 931 μM , respectively); substrate specificity, defined by k_{cat}/K_m , clearly shows preference by the enzyme for the substrate, TBP.

To verify the presence of carbanion in the TBP aldolase-DHAP intermediate, carbanion oxidation by hexacyanoferrate(III) was assayed and showed reduction in the presence of DHAP, FBP, and TBP, although turnover was lower in the presence of substrates (supplemental Table S1). The Michaelis kinetic parameters derived for TBP aldolase substrates in the oxidation reaction were significantly smaller than for the cleavage reaction and indicated equilibration of a rate-limiting step in the carbanion oxidative shunt (supplemental Table S1).

Structure of a Class I TBP Aldolase

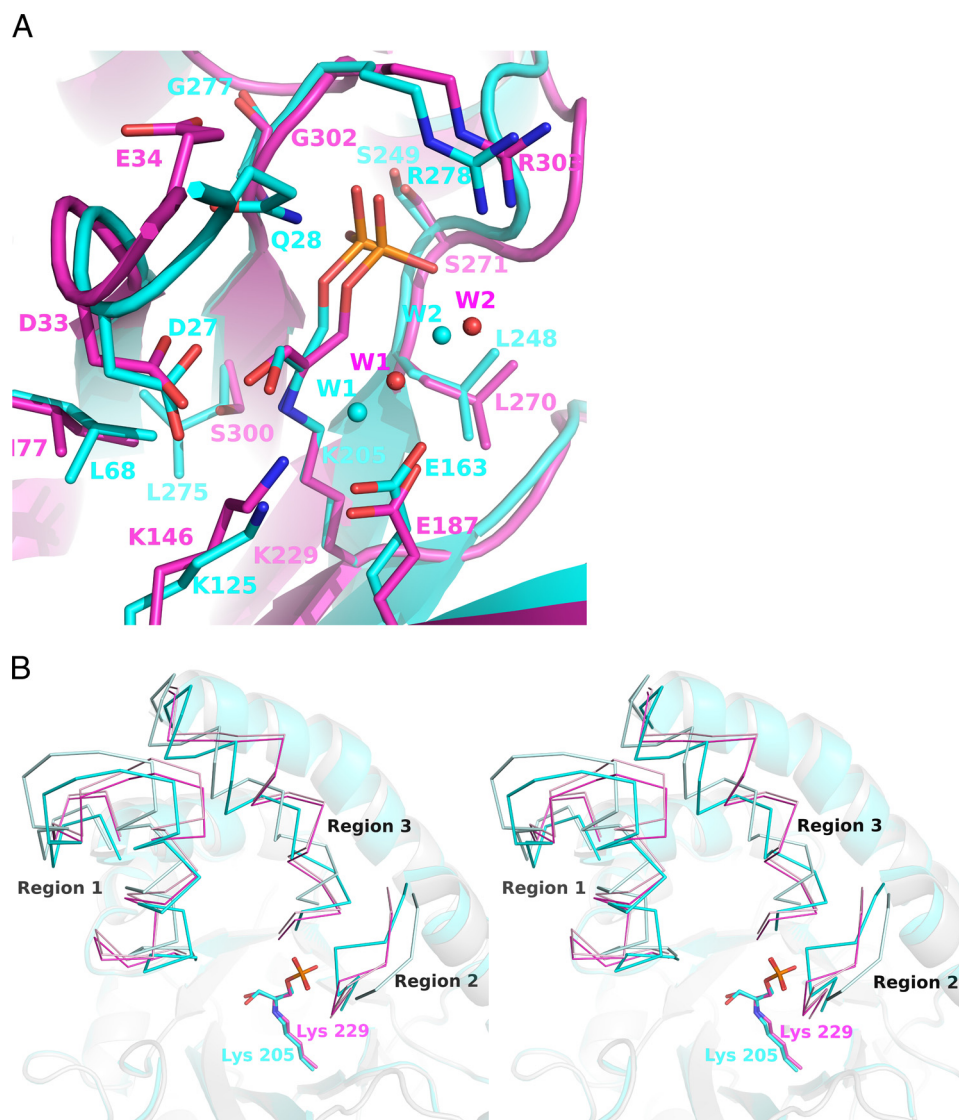


FIGURE 3. *A*, superposition of the DHAP-bound TBP aldolase structure (cyan) with the DHAP bound FBP aldolase (magenta). The superposition shows residues interacting or in close contact with DHAP, which are conserved between the two aldolase structures. The residues Lys²⁰⁵, Glu¹⁶³, Lys¹²⁵, Asp²⁷, Gly²⁷⁷, Arg²⁷⁸, Ser²⁴⁹, and Leu²⁴⁸ in the trapped DHAP-TBP aldolase complex superpose with residues Lys²²⁹, Glu¹⁸⁷, Lys¹⁴⁶, Asp³³, Gly³⁰², Arg³⁰³, Ser²⁷¹, and Leu²⁷⁰ in the DHAP-FBP aldolase complex, respectively. Loci of invariant water molecules, Wat¹ and Wat², in each structure were also conserved. Two notable differences are the replacement of Glu³⁴ and Ser³⁰⁰ in FBP aldolase by Gln²⁸ and Leu²⁷⁵ in the TBP aldolase structure, respectively. *B*, superposition of the crystal structures of native (pale cyan) and DHAP-bound (magenta) FBP aldolase. The regions 1, 2, and 3, which undergo conserved conformational displacement upon ligand binding, are shown as sticks. The overall fold of the DHAP bound TBP and FBP aldolases are shown in a schematic representation.

TABLE 2
Proton exchange of C3 hydrogen positions of DHAP

The rate of proton exchange catalyzed by TBP aldolase of the DHAP C3 hydrogen was measured by the appearance of tritium isotope label as (S)-[3-³H₁]DHAP or (R)-[3-³H₁]DHAP from tritiated water (tritiation) and by the appearance of tritiated water from (S)-[3-³H₁]DHAP and (R)-[3-³H₁]DHAP (detritiation), as described under "Materials and Methods."

TBP aldolase	Total ^b	Tritiation ^a		Detritiation ^a	
		Pro-R ^c	Pro-S ^c	Pro-R	Pro-S
		<i>s</i> ⁻¹		<i>s</i> ⁻¹	
Soluble enzyme	33.1 ± 2.0	14.9 ± 2.4	29.6 ± 6.6	ND ^d	206 ± 23
Control-soluble enzyme ^e	30.9 ± 4.8			ND	219 ± 25
Crystals	15.0 ± 2 × 10 ⁻³	4.0 ± 2 × 10 ⁻³	13.0 ± 2 × 10 ⁻³	ND	0.10 ± 0.03

^a Errors were calculated from at least three experiments, unless otherwise stated.

^b Rate of label incorporation at (S)-[3-³H₁]DHAP and (R)-[3-³H₁]DHAP combined.

^c Labeling of DHAP as (S)-[3-³H₁]DHAP or (R)-[3-³H₁]DHAP was determined using stereospecific detritiation by rabbit muscle aldolase or triose-isomerase, respectively.

^d ND, not detected. Rate of detritiation was statistically insignificant relative to background.

^e Detritiation of (S)-[3-³H₁]DHAP or (R)-[3-³H₁]DHAP previously labeled by TBP aldolase was performed using TBP aldolase.

To evaluate D₂O kinetic solvent isotope effects, enzyme activity measurements were performed in D₂O, and resultant turnover was compared with turnover in H₂O and is shown in supplemental Table S1. A significant isotope effect was observed with the largest $k_{\text{cat}}(\text{H}_2\text{O})/k_{\text{cat}}(\text{D}_2\text{O})$ ratio of 3.3 measured for FBP as substrate compared with 2.3 for TBP.

Proton Exchange—To determine the rate of label exchange at DHAP C3 hydrogen, initial rate velocities were measured in tritiated water to assess label uptake either as (S)-[3-³H₁]DHAP or (R)-[3-³H₁]DHAP and by the appearance of label in tritiated water from (S)-[3-³H₁]DHAP or (R)-[3-³H₁]DHAP. The rates of proton exchange at C3 of DHAP determined at saturation concentrations in solution and crystalline state are shown in Table 2. TBP aldolase labeled both pro-R and pro-S C3 hydrogen positions of DHAP in solution, with an approximate 2-fold kinetic preference for pro-S labeling as compared with pro-R. Detritiation by the enzyme was surprising because it was unable to detritiate label at the pro-R C3 hydrogen position of DHAP; label release was indistinguishable from that measured in the absence of enzyme. A control experiment was performed to confirm this result; DHAP was first labeled using TBP aldolase, and the labeled DHAP was then detritiated again using TBP aldolase. The amount of residual label present as (S)-[3-³H₁]DHAP or (R)-[3-³H₁]DHAP was then measured, and rates are presented

in Table 2. The results show that the enzyme was not capable of significantly detritiating pro-*R*-labeled DHAP although it had effectively labeled the pro-*R* C3 position.

Exchange rates for the crystalline state shown in Table 2 were considerably smaller. Label uptake in TBP aldolase crystals had strong kinetic preference for labeling the pro-*S* C3 hydrogen position of DHAP. The rate of label uptake as (*R*)-[3-³H₁]DHAP is not statistically different from background and indicated a limit on label partitioning of >3:1 in favor of pro-*S* labeling in the crystalline state. Similar to the soluble enzyme, detritiation of label at the pro-*R* C3 hydrogen position of DHAP was not detected in the crystalline enzyme because label release was statistically indistinguishable from background. Both the rate for labeling and detritiation at the pro-*S* DHAP C3 hydrogen in the crystalline state indicate that soaking of TBP aldolase crystals for a period of 5 min with DHAP corresponds to multiple turnovers in both directions and is consistent with exchange occurring under steady state conditions.

The 7-fold greater rate of detritiation in solution compared with tritium label incorporation in Table 2 corresponds to an equilibrium distribution of covalent intermediates on the enzyme where the combined enamine and carbanion population exceeds that of the Schiff base intermediate by ~85:15. In TBP aldolase crystals, although the uncertainties are greater, the exchange rates indicate a similar preference (6.6-fold) for enamine and carbanion populations over the Schiff base. The dominant covalent intermediate trapped on the enzyme in the crystalline state is thus not an imine and is consistent with cryotrapping of a predominant carbanion species in the active site.

DISCUSSION

The structure determination of this class I TBP aldolase has afforded insight into this enzyme's mechanism and evolution. The folding of the polypeptide chain of TBP aldolase, shown in supplemental Fig. S1, corresponds to a (α/β)₈ or triose-phosphate isomerase barrel fold that is typical of class I and II aldolases (44). The extensive conservation of the active site residues and their identical spatial disposition between class I FBP and TBP aldolases is consistent with the hypothesis of divergent evolution from a common ancestor (45). The largest difference between the two aldolases was a loss in TBP aldolase of 23 residues that comprise the flexible C-terminal region in FBP aldolase, which interacts with the active site (11); the remaining differences were associated with conformations of connecting loops between secondary structure elements and a positional shift in helices 5 and 6 to accommodate differential subunit interfaces between the two aldolases. In TBP aldolase, the C terminus position terminates at the end of helix α 11 and is ~20 Å distant from its active site and therefore cannot interact with it. Loss of the C-terminal region in FBP aldolase reduces cleavage activity by ~20-fold (46) and Schiff base-carbanion interconversion by 2 orders of magnitude (47). Thus, although the two aldolases have comparable catalytic activity, the truncation of the C-terminal region in TBP aldolase implies a divergent evolutionary solution to the mechanism of α -proton exchange by the two aldolases.

DHAP Carbanion Intermediate—The trapping of the DHAP enzymatic intermediate clearly demarcated the active site in TBP

aldolase and delineated amino acid residues that are responsible for stabilization of the covalent intermediate. Both structural characterization and proton exchange data at C3 corroborate the identification of the dominant steady state intermediate as the carbanion (Fig. 1B). The carbanion is extensively stabilized by numerous electrostatic interactions and hydrogen bonds with active site residues that are nearly identical to those observed in the enamine complex that was trapped in class I FBP aldolase (Fig. 3). In addition to covalent intermediate formation involving an equivalent lysine residue on each enzyme, the mode of DHAP binding in the active sites of both enzymes is isomorphous and makes use of similar arginine, serine, and glycine residues to grasp the P1 oxyanion while an equivalent aspartate and lysine residues are used to bind the DHAP C3 hydroxyl. A distinctive feature in the FBP aldolase was the preferential enamine stabilization, promoted by Ser³⁰⁰ hydroxyl hydrogen-bonding Lys²²⁹ N ζ that allowed the enzyme to differentiate between enamine and carbanion mesomers (11). The equivalent serine residue is absent in the TBP aldolase active site and is replaced by Leu²⁷⁵. The mesomeric discrimination against the enamine in TBP aldolase is consistent with Leu²⁷⁵ destabilizing the enamine intermediate because the residue cannot engage in hydrogen bond formation with Lys²⁰⁵.

C3 Epimerization—Class I TBP aldolases, contrary to FBP aldolases, lack a flexible C-terminal region capable of mediating *si* face proton transfer at C3 of the carbanion. The active site of TBP aldolase, however, contains two water molecules, Wat¹ and Wat², which are invariant to binding events (Fig. 1A) and are similarly positioned with respect to bound DHAP as two water molecules (similarly designated Wat¹ and Wat²) found in the structure of FBP aldolase (Fig. 3A). Water molecule Wat¹ in TBP aldolase is well positioned *si* face to the DHAP C3 by hydrogen bonding with Glu¹⁶³ and is relatively mobile, whereas water molecule Wat² is tightly bound to the phosphate oxyanion. Wat² is also in close contact with Wat¹, making them well situated to mediate a sequential proton transfer, as was described for FBP aldolase (11). Such a proton exchange role is not inconsistent with the observed kinetic solvent isotope effect and is supported by the virtual identity of active site residues between FBP and TBP aldolases. In FBP aldolase, the P1 phosphate dianion acts as a conjugate base to catalyze proton transfer at physiological pH that is relayed through its invariant water molecule Wat² and activates Wat¹. This activated water molecule, with a slight lateral shift (<1 Å) toward the DHAP C3 carbon in FBP aldolase, would hydrogen-bond with Lys¹⁴⁶ and position it to catalyze stereospecific pro-*S* α -proton transfer in carboxypeptidase-treated FBP aldolase (47). The ability to label C3 pro-*S* hydrogen of DHAP by TBP aldolase would support such a mechanism as water molecule, Wat¹, is positioned within close contact and *si* face with respect to C3. A lateral shift by Wat¹ of ~1 Å enables Lys¹²⁵ to hydrogen-bond Wat¹ and also position it for pro-*S* α -proton transfer.

Labeling of the C3 pro-*R* hydrogen from the *re* face of DHAP cannot be reconciled with a proton transfer mechanism such as that described for *si* face proton exchange at C3. The crystal structure shows no water molecule positioned roughly perpendicular and *re* face with respect to the plane defined by DHAP C1, C2, and C3 that could mediate pro-*R* labeling. A water mol-

Structure of a Class I TBP Aldolase

ecule positioned as the mirror image of Wat¹ with respect to C3 cannot be accommodated because this would result in steric clash with Ala²⁵. Asp²⁷ could act as a conjugate base to catalyze *re* face proton transfer; however, from Fig. 1A, the residue is not well positioned with respect to C3 to mediate proton transfer. Rotations by the Asp²⁷ side chain do not result in an orientation favorable for *re* face proton transfer by Asp²⁷. Furthermore, the trajectory of conformational change by helical region 1 (residues 25–50), which brings Asp²⁷ within hydrogen bonding distance of DHAP C3 hydroxyl, also does not result in a geometry capable of pro-*R* labeling by Asp²⁷ and makes this residue an unlikely candidate for *re* face proton transfer.

Cis-trans Isomerization—Rotation of the hydroxymethyl group of the bound DHAP has been postulated as a mechanism for the apparent C3 epimerization and requires that enolization as well as C–C bond cleavage or synthesis proceed at rates faster than release of the products from the enzyme (48). Isotopic studies on deoxyribose 5-phosphate aldolase have indicated that, during the cleavage of deoxyribose 5-phosphate, rotation of the methyl group of the enzyme-bound acetaldehyde and enolization occurred prior to product release, resulting in an apparent lack of stereospecificity with respect to proton uptake at C2 (equivalent to C3 of a pyruvate lyase substrate) (48). Indeed, proton exchanges in TBP aldolase, shown in Table 2, appear to proceed at rates faster than C–C bond cleavage. Rotation about the equivalent C2–C3 bond in the DHAP intermediate of TBP and FBP aldolases is, however, restricted due to its double bond character and limits the rotamers to the two discrete isomers: *E*, where the DHAP O3 hydroxyl is oriented *cis* to the DHAP C2–Lys²⁰⁵ N ζ bond, and *Z*, where the orientation is *trans*. Their relative populations depend on the active site stabilization of each isomer, and their rate of interconversion is determined by the height of the rotational barrier, which depends on the extent of double bond character at C2–C3. The rotational barrier would be greater in the enamine than in the carbanion, which has reduced C2–C3 double character.

Fig. 1, A and B, shows the DHAP intermediate bound as the *E* isomer, whereas Fig. 4 shows a possible conformation for the *Z* isomer as modeled from the *E* isomer. Stabilization of the DHAP C3 hydroxyl in the *E* isomer implicates three hydrogen bonds with active residues Asp²⁷ and Lys¹²⁵. The DHAP C3 hydroxyl, by adopting a *trans* configuration in Fig. 4, forms a hydrogen bond with DHAP O1 (2.4–2.6 Å) that would be further stabilized by hydrogen bonding with Gln²⁸. The observed 2:1 ratio in the rates of pro-*S* and pro-*R* labeling at C3 of DHAP in TBP aldolase is consistent with a mechanism of stereofacial *si* face proton transfer at C3 in both *E* and *Z* isomers with more extensive hydrogen bonding stabilizing the *E* isomer. Preferential stabilization of carbanion mesomer by the enzyme would favor the requisite *cis-trans* isomerization about the C2–C3 bond due to its reduced double bond character in the carbanion. In FBP aldolase, the presence of Glu³⁴, equivalent to Gln²⁸ in TBP aldolase (Fig. 3A), would not favor hydrogen bonding with DHAP O3 hydroxyl in the *Z* isomer compared with TBP aldolase, because such an interaction with Glu³⁴ would simultaneously make a repulsive interaction with DHAP O1. Furthermore, the greater double bond character of the C2–C3 bond in the enamine heightens the barrier to *cis-trans* isomer-

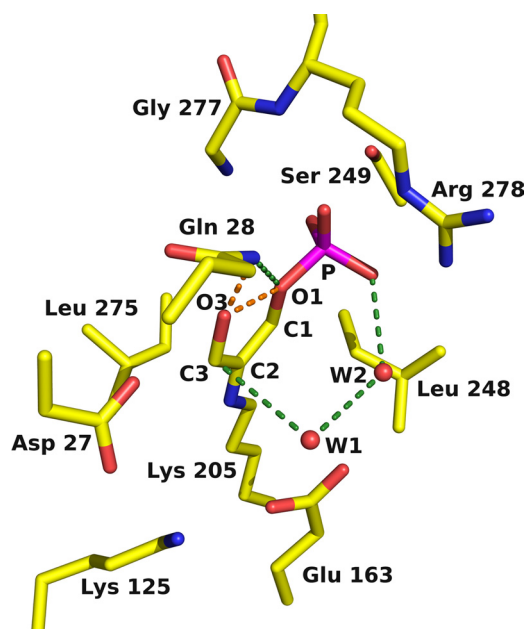


FIGURE 4. Isomerization of the carbanion enzymatic intermediate formed with DHAP in the TBP aldolase active site. The DHAP C3 hydroxyl, which is predominantly bound as the *E* isomer or *cis* configuration, is shown modeled binding as the *Z* isomer or *trans* configuration with respect to the DHAP C2–Lys²⁰⁵ N ζ bond. The *Z* isomer results in formation of two hydrogen bonds (shown in orange) by DHAP C3 hydroxyl with DHAP O1 and Gln²⁸ and would allow protonation of the pro-*R* position of DHAP C3 by the same stereofacial proton transfer mechanism, implicating water molecules Wat¹ and Wat² as used for protonation of the pro-*S* position of DHAP C3 in Figs. 1A and 3A. Gln²⁸ is positioned by its two hydrogen bonds made with the DHAP ester oxygen and oxyanion. Pertinent hydrogen bonds or close contacts present in the *E* isomer are shown in green. Such geometry is feasible for *sp*² hybridization at C3 in the carbanion, whereas *sp*³ hybridization in the Schiff base or iminium intermediate would result in an unacceptable close contact between DHAP C3 hydroxyl and DHAP O1.

ization. Together, these considerations explain the inability to detect pro-*R* labeling of the DHAP C3 hydrogen in FBP aldolase (16). The loss of stereospecific labeling at C3 in TBP aldolase is thus a likely consequence of *cis-trans* isomerization of the carbanion promoted by Gln²⁸ and Leu²⁷⁵. From an evolutionary perspective, C3 epimerization in class I DHAP-dependent aldolases would be based on a conserved stereospecific proton transfer mechanism exploiting *cis-trans* isomerization in the carbanion intermediate.

The preferential labeling in the crystalline state of the pro-*S* C3 hydrogen with respect to the pro-*R* DHAP C3 hydrogen of >3:1 implies a population for the *Z* isomer that would have occupancy of less than 25% in the crystal structure and which would make it technically challenging to observe above the noise level in the electron density map. The small exchange rates in the crystalline state as well as the labeling pattern would argue that crystal lattice packing decreases exchange rates and differentially stabilizes *Z* and *E* isomer populations with respect to solution. Indeed, in all subunits, conformational mobile regions 1 and 2 that respond to DHAP binding participate in crystal packing contacts and thus could redirect *Z* and *E* isomer stability and the barrier height of *cis-trans* isomerization. Fluctuations along the conformational trajectory made by region 1 upon DHAP binding, which could disrupt Asp²⁷ hydrogen bond formation with DHAP O3 and facilitate *cis-trans* isomerization, also would be hindered by the crystal lattice packing.

The *Z* isomer configuration shown in Fig. 4 is however only possible if the carbanion intermediate has sp^2 hybridization at C3 because sp^3 hybridization at C3 would result in an unacceptable close contact between DHAP C3 hydroxyl and DHAP O1 in this isomer. A planar carbanion center is favored because the nucleophile is adjacent to the DHAP C2- Lys²⁰⁵ N ζ double bond that affords conjugative stabilization. The destabilization of the *Z* isomer in the Schiff base, due to its sp^3 hybridization at C3, would be consistent with a very low rate of pro-*R* detritiation at C3, which was not detected, in comparison with a very high rate of pro-*S* detritiation at C3, as shown in Table 2. The inhibition of the Schiff base to carbanion interconversion and a kinetic preference for pro-*S* labeling indicate a transaldolase rather than aldolase activity toward sorbose bisphosphate and psicose bisphosphate as substrates.

Induced Conformational Changes—In Fig. 2, three regions in the native enzyme are shown to undergo small yet significant conformational changes upon active site binding by DHAP. The conformational changes consist of rigid body movements induced by DHAP that serve to stabilize the DHAP-enzyme intermediate and are very akin to those observed in the structures of rabbit muscle aldolase bound to DHAP and FBP (11, 27). Both FBP and TBP aldolases respond to active site binding by identical asymmetrical active site narrowing, implicating equivalent α -helices and regions of the β -turn flanking the active site, as shown in Fig. 3B. Conformational displacements by these secondary structure features serve in both cases to bind the DHAP phosphate oxyanion and C3 hydroxyl. The low sequence homology between those two class I aldolases that are functionally very similar suggests not only that the α/β barrel platform is functionally robust and able to tolerate considerable sequence divergence but also that the conformational changes requisite to binding are strongly conserved, being invariant to the same degree of sequence divergence.

The conformational changes observed in TBP aldolase may thus represent the molecular basis enabling the LacD.1 paralogue of TBP aldolase in *S. pyogenes* and to which TBP aldolase is highly homologous (73% identical and 86% similar) to act as a putative metabolic sensor that regulates global transcription of virulence genes in *S. pyogenes* (49, 50). Sequence differences between the two paralogues are largely at the level of surface-exposed residues whereas active site residues are conserved and implicitly support the hypothesis of homologous conformational changes in LacD.1 triggered by active site binding. All residues in *S. pyogenes* LacD.2 found proximal to the bound DHAP intermediate (namely Asp²⁷, Gln²⁸, Arg²⁹, Glu⁹², Lys¹²⁵, Glu¹⁶³, Lys²⁰⁵, Leu²⁷⁵, Gly²⁷⁷, and Arg²⁷⁸) are sequence-conserved and spatially conserved in the computed LacD.1 model. Furthermore, residues vicinal to the active site were also conserved both in identity and position. Experimental data indicate that the role of LacD.1 depends on substrate recognition, especially on DHAP, but not on enzymatic activity and is most sensitive to changes in DHAP levels (49). Under conditions of high glycolysis, product binding by DHAP could thus induce a conformational change in LacD.1. Indirect evidence suggests that LacD.1 sequesters a regulatory partner and, by inhibiting it from activating its target genes, triggers virulence gene expression (49). Interference with or exploitation of these conforma-

tional changes in *S. pyogenes* would represent a novel target to inhibit virulence of this versatile human pathogen, which is the causative agent of numerous human diseases, ranging from pharyngitis and impetigo to the often fatal necrotizing fasciitis and septicemia (51). The substrate ambiguity benefits the simple fermentative energy metabolism of *S. pyogenes* by allowing it to respond and adapt to environmental alterations in carbon sources (49).

Acknowledgments—Work was carried out in part at beamlines X12B, X25, and X29 of the National Synchrotron Light Source (supported principally by the Offices of Biological and Environmental Research and of Basic Energy Sciences of the United States Department of Energy and the National Center for Research Resources of the National Institutes of Health). Assistance by beamline personnel, Drs. L. Flaks, D. K. Schneider, A. Soares, A. Héroux, and H. Robinson, is gratefully acknowledged. The help of Laurent Cappadoccia in data collection was particularly appreciated. Critical reading of the manuscript by Dr. Casimir Blonski was also appreciated. Tagatose 1,6-bisphosphate was a generous gift of Dr. W. Fessner.

REFERENCES

- Suri, J. T., Mitsumori, S., Albertshofer, K., Tanaka, F., and Barbas, C. F., 3rd (2006) *J. Org. Chem.* **71**, 3822–3828
- Takayama, S., McGarvey, G. J., and Wong, C. H. (1997) *Annu. Rev. Microbiol.* **51**, 285–310
- Fessner, W. D. (1998) *Curr. Opin. Chem. Biol.* **2**, 85–97
- Wong, C. H., Whitesides, G. M. (1994) *Enzymes in Synthetic Organic Chemistry*, pp. 195–232, 1st Ed., Elsevier Science Publishing Co., Inc., New York
- Bissett, D. L., and Anderson, R. L. (1980) *J. Biol. Chem.* **255**, 8750–8755
- Lee, J. H., Bae, J., Kim, D., Choi, Y., Im, Y. J., Koh, S., Kim, J. S., Kim, M. K., Kang, G. B., Hong, S. I., Lee, D. S., and Eom, S. H. (2006) *Biochem. Biophys. Res. Commun.* **347**, 616–625
- Grazi, E., Rowley, P. T., Cheng, T., Tchola, O., and Horecker, B. L. (1962) *Biochem. Biophys. Res. Commun.* **9**, 38–43
- Kobashi, K., Lai, C. Y., and Horecker, B. L. (1966) *Arch. Biochem. Biophys.* **117**, 437–444
- Kobes, R. D., Simpson, R. T., Vallee, R. L., and Rutter, W. J. (1969) *Biochemistry* **8**, 585–588
- Harris, C. E., Kobes, R. D., Teller, D. C., and Rutter, W. J. (1969) *Biochemistry* **8**, 2442–2454
- St-Jean, M., and Sygusch, J. (2007) *J. Biol. Chem.* **282**, 31028–31037
- Rose, I. A. (1969) *Comprehensive Biochemistry*, pp. 93–161, Vol. 17 (Florkin, M., and Stoltz, E. H., eds) Elsevier Science Publishing Co., Inc., New York
- Jencks, W. P. (1987), *Catalysis in Chemistry and Enzymology*, pp. 120–127, Courier Dover Publications, New York
- Grazi, E., Cheng, T., and Horecker, B. L. (1962) *Biochem. Biophys. Res. Commun.* **7**, 250–253
- Rose, I. A., and Rieder, S. V. (1958) *J. Biol. Chem.* **231**, 315–329
- Rose, I. A. (1958) *J. Am. Chem. Soc.* **80**, 5835–5836
- Chiu, T. H., and Feingold, D. S. (1965) *Biochem. Biophys. Res. Commun.* **19**, 511–516
- Chiu, T. H., and Feingold, D. S. (1969) *Biochemistry* **8**, 98–108
- Kobes, R. D., and Dekker, K. E. (1969) *J. Biol. Chem.* **244**, 1919–1925
- Meloche, H. P., and Mehler, L. (1973) *J. Biol. Chem.* **248**, 6333–6338
- Espelt, L., Bujons, J., Parella, T., Calveras, J., Joglar, J., Delgado, A., and Clapés, P. (2005) *Chemistry* **11**, 1392–1401
- Zgiby, S. M., Thomson, G. J., Qamar, S., and Berry, A. (2000) *Eur. J. Biochem.* **267**, 1858–1868
- Williams, G. J., Domann, S., Nelson, A., and Berry, A. (2003) *Proc. Natl. Acad. Sci. U.S.A.* **100**, 3143–3148
- Sygusch, J., Beaudry, D., and Allaire, M. (1987) *Proc. Natl. Acad. Sci. U.S.A.*

Structure of a Class I TBP Aldolase

- 84, 7846–7850
25. Chudzik, D. M., Michels, P. A., de Walque, S., and Hol, W. G. (2000) *J. Mol. Biol.* **300**, 697–707
 26. Dalby, A. R., Tolan, D. R., and Littlechild, J. A. (2001) *Acta Crystallogr. D Biol. Crystallogr.* **57**, 1526–1533
 27. St-Jean, M., Lafrance-Vanasse, J., Liotard, B., and Sygusch, J. (2005) *J. Biol. Chem.* **280**, 27262–27270
 28. Liotard, B., and Sygusch, J. (2004) *Acta Crystallogr. D* **60**, 528–530
 29. Racker, E. (1947) *J. Biol. Chem.* **167**, 843–854
 30. Otwinowski, Z., and Minor, W. (1997) *Methods Enzymol.* **276**, 307–326
 31. Terwilliger, T. C., and Berendzen, J. (1999) *Acta Crystallogr. D* **55**, 849–861
 32. Terwilliger, T. C. (2000) *Acta Crystallogr. D* **56**, 965–972
 33. Jones, T. A., Zou, J. Y., Cowan, S. W., and Kjeldgaard, M. (1991) *Acta Crystallogr. A* **47**, 110–119
 34. Brünger, A. T., Adams, P. D., Clore, G. M., DeLano, W. L., Gros, P., Grosse-Kunstleve, R. W., Jiang, J. S., Kuszewski, J., Nilges, M., Pannu, N. S., Read, R. J., Rice, L. M., Simonson, T., and Warren, G. L. (1998) *Acta Crystallogr. D* **54**, 905–921
 35. Adams, P. D., Grosse-Kunstleve, R. W., Hung, L. W., Ioerger, T. R., McCoy, A. J., Moriarty, N. W., Read, R. J., Sacchettini, J. C., Sauter, N. K., and Terwilliger, T. C. (2002) *Acta Crystallogr. D* **58**, 1948–1954
 36. Emsley, P., and Cowtan, K. (2004) *Acta Crystallogr. D* **60**, 2126–2132
 37. Schüttelkopf, A. W., and van Aalten, D. M. (2004) *Acta Crystallogr. D Biol. Crystallogr.* **60**, 1355–1363
 38. Weiss, M. (2001) *J. Appl. Crystallogr.* **34**, 130–135
 39. Collaborative Computational Project 4 (1994) *Acta Crystallogr. D* **50**, 760–763
 40. Diamond, R. (1992) *Protein Sci.* **1**, 1279–1287
 41. DeLano, W. L. (2002) *The PyMOL Molecular Graphics System*, DeLano Scientific LLC, San Carlos, CA
 42. Holm, L., Kääriäinen, S., Rosenström, P., and Schenkel, A. (2008) *Bioinformatics* **24**, 2780–2781
 43. Guex, N., and Peitsch, M. C. (1997) *Electrophoresis* **18**, 2714–2723
 44. Lorentzen, E., Siebers, B., Hensel, R., and Pohl, E. (2004) *Biochem. Soc. Trans.* **32**, 259–263
 45. Wierenga, R. K. (2001) *FEBS Lett.* **492**, 193–198
 46. Spolter, P. D., Adelman, R. C., and Weinhouse, S. (1965) *J. Biol. Chem.* **240**, 1327–1337
 47. Rutter, W. J., Richards, O. C., and Woodfin, B. M. (1961) *J. Biol. Chem.* **236**, 3193–3197
 48. Corina, D. L., and Wilton, D. C. (1976) *Biochem. J.* **157**, 573–576
 49. Loughman, J. A., and Caparon, M. G. (2007) *Mol. Microbiol.* **64**, 269–280
 50. Loughman, J. A., and Caparon, M. G. (2006) *EMBO J.* **25**, 5414–5422
 51. Cunningham, M. W. (2000) *Clin. Microbiol. Rev.* **13**, 470–511

Enzymology:

**Structure of a Class I
Tagatose-1,6-bisphosphate Aldolase:
INVESTIGATION INTO AN APPARENT
LOSS OF STEREOSPECIFICITY**

ENZYMOLOGY

Clotilde LowKam, Brigitte Liotard and Jurgen
Sygusch

J. Biol. Chem. 2010, 285:21143-21152.

doi: 10.1074/jbc.M109.080358 originally published online April 28, 2010

Access the most updated version of this article at doi: [10.1074/jbc.M109.080358](https://doi.org/10.1074/jbc.M109.080358)

Find articles, minireviews, Reflections and Classics on similar topics on the [JBC Affinity Sites](#).

Alerts:

- [When this article is cited](#)
- [When a correction for this article is posted](#)

[Click here](#) to choose from all of JBC's e-mail alerts

Supplemental material:

<http://www.jbc.org/content/suppl/2010/04/28/M109.080358.DC1.html>

This article cites 48 references, 14 of which can be accessed free at
<http://www.jbc.org/content/285/27/21143.full.html#ref-list-1>